HHS Public Access

Author manuscript

ACS Nano. Author manuscript; available in PMC 2016 December 14.

Published in final edited form as:

ACS Nano. 2016 April 26; 10(4): 4119–4126. doi:10.1021/acsnano.5b07360.

Tobacco Mosaic Virus Delivery of Phenanthriplatin for Cancer therapy

Anna E. Czapar[§], **Yao-Rong Zheng**[†], **Imogen A. Riddell**[†], **Sourabh Shukla**[‡], **Samuel G. Awuah**[†], **Stephen J. Lippard**[*,†], and **Nicole F. Steinmetz**[‡,*,||,⊥,#,∇]

[§]Department of Pathology, Case Western Reserve University, Cleveland, Ohio 44118, United States

[‡]Department of Biomedical Engineering, Case Western Reserve University, Cleveland, Ohio 44118, United States

[||]Department of Radiology, Case Western Reserve University, Cleveland, Ohio 44118, United States

[⊥]Department of Materials Science and Engineering, Case Western Reserve University, Cleveland, Ohio 44118, United States

[#]Department of Macromolecular Science and Engineering, Case Western Reserve University, Cleveland, Ohio 44118, United States

[∇]Case Comprehensive Cancer Center, Case Western Reserve University, Cleveland, Ohio 44118, United States

[†]Department of Chemistry, Massachusetts Institute of Technology, Cambridge, Massachusetts 02139, United States

Abstract

Phenanthriplatin, *cis*-[Pt(NH_3)$_2$Cl(phenanthridine)](NO_3), is a cationic monofunctional DNA-binding platinum(II) anticancer drug candidate with unusual potency and cellular response profiles. Its *in vivo* efficacy has not yet been demonstrated, highlighting the need for a delivery system. Here we report tobacco mosaic virus (TMV) as a delivery system for phenanthriplatin. TMV forms hollow nanotubes with a polyanionic interior surface; capitalizing on this native structure, we developed a one-step phenanthriplatin loading protocol. Phenanthriplatin release from the carrier is induced in acidic environments. This delivery system, designated PhenPt-TMV, exhibits matched efficacy in a cancer cell panel compared to free phenanthriplatin. *In vivo* tumor delivery and efficacy were confirmed using a mouse model of triple negative breast cancer. Tumors treated with PhenPt-TMV were 4× smaller than tumors treated with free phenanthriplatin or cisplatin, owing to increased accumulation of phenanthriplatin within the tumor tissue. The biology-derived TMV delivery system may facilitate translation of phenanthriplatin into the clinic.

Graphical Abstract

[*]Corresponding Authors: nicole.steinmetz@case.edu, lippard@mit.edu.

The authors declare no competing financial interest.

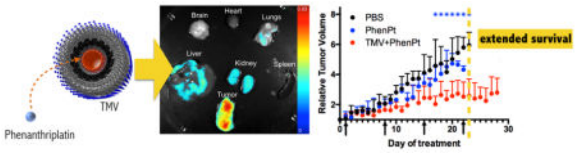

Keywords

cancer therapy; metals in medicine; nanotechnology; drug delivery; tobacco mosaic virus

Platinum-based anticancer agents are used to treat over half the cancer patients receiving chemotherapy, but their clinical utility suffers from dose-limiting toxicity.[1] Another impediment is the development of drug resistance as a result of microenvironmental selection pressures resulting in incomplete cell kill and promoting the growth and recurrence of cancer in a therapy-resistant form.[2] Drug delivery approaches hold the promise to overcome these challenges, because drug carriers have better safety profiles than free drugs and enable tissue-specific targeting and intracellular delivery. The development of platinum-based nanoparticle carriers, however, must overcome challenges that can limit the potency of the drug. For example, liposomal formulations of cisplatin (SPI-77) afford no improvement in clinical efficacy, probably owing to the retention of cisplatin within the nanoparticle.[3]

In the present work we investigated a plant virus-based nanoparticle to deliver the highly potent platinum anticancer agent, *cis*-[Pt(NH_3)$_2$(phenanthridine)Cl](NO_3), or phenanthriplatin.[4] Phenanthriplatin is a monofunctional Pt(II) compound with a distinct tumor cell profile compared to classical platinum drugs (NCI-60 screen, *inter alia*) and much greater (up to 40-fold) potency.[4–7] However, phenanthriplatin performs no better *in vivo* than contemporary treatments such as cisplatin, highlighting the need for a more effective delivery system for the compound (*vide infra*).

Our drug delivery system is produced using the nucleoprotein components of tobacco mosaic virus (TMV), a plant virus-based nanoparticle platform. The application of mammalian viruses in gene delivery and oncolytic virus therapy has already been realized.[8,9] Plant virus-based platforms offer an attractive alternative, because plant viruses do not replicate in or infect mammals. TMV displays good blood and tissue biocompati-bility.[10] The proteinaceous carrier is cleared within hours from nontarget organs, making this biodegradable platform a promising strategy for drug delivery.

The high-aspect-ratio (AR), or length divided by diameter, of cylindrical TMV confers additional advantages. Native TMV measures 300 × 18 nm,[11] and therefore the AR = 16.7. High-AR nanoparticles are advantageous for drug delivery, typically conveying favorable biodistribution and tumor homing properties.[12,13] AR engineering provides a mechanism for immune evasion and increases tumor-targeting properties.[11] We previously demonstrated the utility of TMV as a contrast agent enabling delineation of molecular signatures *in vivo* aiding diagnosis and prognosis.[14] In this work we explore TMV as a drug delivery system to enable phenanthriplatin therapy targeting cancer.

RESULTS AND DISCUSSION

Synthesis and Characterization of TMV-Encapsulated Phenanthriplatin

TMV was propagated and purified from *Nicotiana benthamiana* plants at yields of around 10 mg per gram infected leaf tissue; methods are as previously reported.[15] Phenanthriplatin was synthesized as described previously.[4]

Each TMV nanorod consists of 2130 identical copies of a coat protein unit arranged helically around a single-stranded RNA molecule, creating an accessible 4 nm-wide central channel (Figure 1). TMV has served as a model system in plant pathology and structural biology since the early 1900s; its structure is well-defined.[16] The protein-based scaffold provides a template that enables highly precise insertion of guest molecules through region-specific targeting of solvent-exposed surface groups. Bioconjugate chemistry targeting internal glutamic acids and external tyrosine residues is well established, and carbodiimide, diazonium, and *N*-hydroxysuccinimide reagents can be used to introduce alkyne or benzaldehyde ligands for subsequent derivatization using Cu(I)-catalyzed azide–alkyne cycloaddition,[15,17] hydrazone coupling, or oxime condensation.[18,19] We previously showed that covalent strategies enable incorporation of contrast agents and/or peptide ligands.[14] However, these methods involve multiple synthetic steps requiring repeated purification from excess reagents, thereby lowering the yield of the final product. These technical challenges are not an issue in the present case, where a simple solution protocol involving straightforward nano-encapsulation of the cationic guest in the anionic tubular environment of the virus afforded the desired phenanthriplatin-loaded TMV formulation (PhenPt-TMV), Figure 1.

The inner and outer surfaces of TMV provide distinct chemical environments. The interior channel affords a high density of negative surface charges from the 4260 glutamic acids (Glu 97 and 106, see Figure 1), whereas no carboxylates are present on the exterior TMV surface. We anticipated that this high-density glutamic acid matrix would favor encapsulation of positively charged therapeutics, specifically, phenanthriplatin (Figure 1).

To test whether the association of phenanthriplatin and TMV was electrostatically driven, both phenanthriplatin ($PhenPt^{+}$, Figure 1) and its aquated form, ($PhenPt^{2+}$, Figure 1), obtained through reaction with $AgNO_3$, were allowed to react with TMV by mixing in solution. Following purification of PhenPt-TMV using ultracentrifugation to remove excess reagents, the Pt content per TMV particle was determined by inductively coupled plasma mass spectroscopy (ICP-MS). The results indicate that a 30-min loading with 2000 ± 200 phenanthriplatin cations per TMV when using $PhenPt^{2+}$, supporting the conclusion that binding occurs to the carboxylate groups lining the inner core of the virus (Figure 2C). The 2+ charge of $PhenPt^{2+}$ compensates two carboxylate amino acid side chains lining the interior surface of the virus. $PhenPt^{+}$ resulted in fewer than 1000 phenanthriplatin cations per nanorod. Further studies are in progress to elucidate the reason for this value.

To confirm that phenanthriplatin loading requires the internal carboxylates, we conjugated the positively charged cyanine5 dye (Cy5) to the interior carboxylates using a combination of carbodiimide coupling to introduce an alkyne followed by Cu(I)-catalyzed azide–alkyne

cycloaddition of an azide-functional Cy5 (“click” chemistry). The reactions and Cy5-TMV particle characterization were performed as previously described.[14] Attempted phenanthriplatin loading of the Cy5-modified TMV did not yield any detectable encapsulation as measured by ICP-MS, supporting exclusively interior loading through electrostatic gating and, most likely, coordination of the carboxylates to platinum atoms.

Transmission electron microscopy (TEM) imaging of PhenPt-TMV confirms that the nanorods remain structurally sound after phenanthriplatin loading (Figure 2A). Dynamic light scattering and zeta potential measurements indicate no statistically significant differences comparing native TMV and PhenPt-TMV, further supporting interior loading of the compound (Figure 2B).

Next, we evaluated the phenanthriplatin release profile. PhenPt-TMV was prepared as described and dialyzed against PBS at pH 7.4 or sodium acetate buffer at pH 5.0. These conditions were chosen to mimic the acidic lysosomal and tumor microenvironments[20] compared to physiological pH in blood. Increased release rates were apparent at low pH in solutions of PhenPt-TMV formulations. Approximately half the phenanthriplatin content was released within the first hour, release of the remaining cation occurred at 24 h. In stark contrast, release at pH 7.4 was significantly slower. About 50–60% of the phenanthriplatin content was released after 24 h reaching a plateau, and complete release was not observed over the 72 h time course. Although the PhenPt-TMV complex lacks long-term stability, the one-step loading process facilitates its formation immediately prior to use.

The rapid release of phenanthriplatin in acidic environments may be explained by protonation of the carboxylic acids, which destabilizes the PhenPt-TMV complex. This finding is important considering that previous approaches to drug delivery of platinum compounds failed in the clinic owing to lack of drug release, an example being trials evaluating liposomal formulations of cisplatin (SPI-77).[3] Our data indicate that the virally encapsulated materials efficiently release their cargo; at the same time, stability at physiological pH is expected to protect against premature release while in circulation, thereby preventing off-target systemic effects.

PhenPt-TMV cytotoxicity and cell interactions *in vitro*

The anticancer activity of PhenPt-TMV was evaluated using a panel of cancer cells and compared to those of unencapsulated phenanthriplatin and cisplatin. The data indicate that PhenPt-TMV maintained efficacy compared to free phenanthriplatin. Both PhenPt-TMV and phenanthriplatin outperformed cisplatin in cancer cell lines of breast, ovarian, and pancreatic origin (Figure 3A,B). Whereas the IC_{50} values for cisplatin ranged from 0.88 μM to >20 μM, the IC_{50} values for phenanthriplatin and PhenPt-TMV ranged from 0.29 to 3.59 μM, depending on cell type. Free phenanthriplatin and PhenPt-TMV showed enhanced efficacy in ovarian cancer cells resistant to cisplatin treatment.[21] Enhanced efficacy was also observed using primary patient cells OV81.2.[22] Native TMV showed no cytotoxicity (Figure 3B), attesting to its biocompatibility.

Next, we determined cell interactions and the intracellular distribution of PhenPt comparing free and TMV-delivered material (Figure 3C–E). Using MDA-MB-231 cells and flow

cytometry protocols, we determined that TMV efficiently interacts with cancer cells (Figure 3C). This result is consistent with TMV cellular trafficking experiments (Figure 4) and previous reports that TMV is internalized by cancer cells through endocytosis and targeted to the endolysosome, where the free drug is released following degradation of the proteinaceous carrier.[23,24] Assessment of the intracellular distribution of platinum content revealed that 24 h after exposure of A2780 cells to PhenPt-TMV phenanthriplatin was detected in the nucleus at levels comparable to those obtained with free phenanthriplatin (Figure 3D,E). These results are consistent with PhenPt-TMV release from the virus intracellularly, where the carboxylic acids become protonated leading to phenanthriplatin release (see Figure 2D). Following initial release, the acidic environment and the presence of hydrolases and proteases will degrade the proteinaceous carrier over time, further releasing membrane permeable phenanthriplatin.

PhenPt-TMV *in Vivo* Efficacy and Biodistribution

The *in vivo* properties of PhenPt-TMV were assessed using a mouse model of triple negative breast cancer, MDA-MB-231 xenografts induced in NCR nu/nu mice. Weekly intravenous bolus injections using a dose of 1.0 mg/kg phenanthriplatin commenced when tumors reached a volume of 250–300 mm^3. Groups were treated with PhenPt-TMV, TMV, phenanthriplatin, or cisplatin (dosage was normalized to total platinum content), and a control group received PBS. PhenPt-TMV was freshly prepared, and the Pt content was confirmed by ICP-MS, prior to each injection. Disease burden, assessed by tumor volume, was monitored for 30 days (Figure 5). Side effects were evaluated daily by examining the physical condition, body weight, and behavior of the animals.

The tumor treatment study showed that PhenPt-TMV outperformed free phenanthriplatin as well as the drug cisplatin, which were ineffective at a 1 mg/kg dose. Also, TMV treatment showed no statistically significant difference compared to PBS-treated control groups. Tumor growth rates of PhenPt-TMV-treated animals were significantly slower compared to treatment with free phenanthriplatin or TMV, indicating successful targeting and efficacy. PhenPt-TMV treated tumors were 4× smaller compared to tumors in the control groups. Free phenanthriplatin and TMV treatment had no effect (Figure 5A,C), and significant tumor burden, defined by volumes exceeding 10% of the animal's body weight, required termination of the experiment before completion of the study. Efficacy was also confirmed by histology. The intra-tumoral effects of PhenPt-TMV were evaluated using histology and hematoxylin and eosin (H&E) staining following completion of the study (Figure 6). In addition to a reduction in overall tumor volume, tumors treated with PhenPt-TMV showed a reduced cellularity and apparent nuclear condensation, supporting intratumoral apoptosis caused by the action of phenanthriplatin within the tumor.

Cisplatin was less effective in the *in vitro* cell culture and *in vivo* assays performed here. In contrast, phenanthriplatin is highly effective in cell culture (Figure 3), but lacks *in vivo* efficacy, highlighting the great value in the present viral delivery system. The TMV-based carrier appears to be a most promising candidate toward the goal of moving phenanthriplatin to the clinic.

The biodistribution of PhenPt-TMV, including co-localization of phenanthriplatin and TMV, was evaluated 24 h post-administration using a combination of fluorescent imaging (Maestro Imager) and elemental analysis (Graphite Furnace Atomic Absorption Spectroscopy). To enable fluorescence imaging, TMV was labeled with sulfo-Cy5 dye at exterior tyrosine side chains as previously described,[14] then loaded with phenanthriplatin. The phenanthriplatin loading efficiency was unaffected by exterior modification by the fluorophore, further supporting interior loading of this drug candidate. Imaging and region of interest (ROI) analysis indicated that PhenPt-TMV indeed targeted the tumor tissue (Figure 7A,B). This result can be explained by passive homing based on the enhanced permeability and retention (EPR) effect. The neovasculature required by rapidly growing tumors is more permeable than that of surrounding healthy tissue, leading to preferential accumulation of nanoparticles in tumor tissue.[25] High-AR materials, such as TMV, exhibit increased tumor homing properties based on increased margination and tissue penetration properties.[12,13]

Maestro imaging indicated that PhenPt-TMV also reaches nontarget organs. This biodistribution is expected from our earlier studies; proteinaceous nanoparticles are cleared through a combination of renal filtration and sequestration in organs of the mononuclear phagocyte system, the liver and spleen.[10,26]

Platinum elemental analysis (Figure 7C,D) also confirmed successful delivery to the tumor tissue as well as clearance through the liver and kidneys. Over the course of the study, mice treated with PhenPt-TMV did not show any weight loss (Figure 8A) or behavioral changes, indicating that the formulation is well tolerated with no apparent toxicity.

Overall, the biodistribution data support the efficacy study; the TMV delivery system targets the potent material to tumor tissue, enabling treatment. Systemic administration of phenanthriplatin is ineffective.

The potential toxicology of PhenPt-TMV treatment compared to control groups was assessed by body weight monitoring, liver enzyme testing, and histology of liver and kidneys (Figure 8). Balb/c mice were treated via intravenous injection with PBS, TMV, phenanthriplatin, or PhenPt-TMV at the same dosing schedule used for the efficacy studies (1.0 mg/kg phenanthriplatin or PhenPt-TMV, normalized for platinum content and TMV). Blood was collected by retro-orbital bleeds, 24 h following injection, and aspartate aminotransferase (AST) and alanine aminotransferase (ALT) levels were assessed (Figure 8B). No significant changes in the levels of either enzyme were observed in the TMV group, however, both free PhenPt and PhenPt-TMV groups showed a significant increase in AST when compared to PBS. An increase in ALT level was observed for the PhenPt-TMV group; however, values recorded were within the normal range for this mouse breed (Charles River). Although ALT is a specific liver viability indicator, AST is less specific to liver. No significant changes in ALT levels were observed, consistent with histology indicating no apparent toxicity (Figure 8B,C). The increased AST levels may point to adverse effects induced in other organs, such as the kidneys.[27] Indeed, histology staining indicated necrosis of epithelia on the proximal tubules as well as narrowing of the lumen (Figure 8C), observed for phenanthriplatin and PhenPt-TMV treated groups. The data therefore indicate potential kidney damage, a common side effect for platinum-based chemotherapeutics, typically

managed in human patients by hydration, sometimes accompanied by a diuretic.[1] Although these studies point to the need for more detailed toxicology studies to determine the maximum tolerated dose, the lack of weight loss or changes in activity level of the treated animals suggests that adverse effects may be manageable throughout the course of treatment. Nephrotoxicity may also be reduced through coating of TMV with polyethylene glycol, a polymer that decreases clearance of viral nanoparticles through the kidney.[26]

Another important future direction is the consideration of the potential immunotoxicity. Immune cell interactions of nanocarriers and delivered therapeutics are a double-edged sword, and more research is required to gain a better understanding of the benefits and side effects. For example, macrophages can act as a depot for drug carriers.[28] We recently demonstrated that plant virus carriers can stimulate a potent antitumor response through activation of the innate immune system.[29] Here we observe a slight delay in tumor growth in the TMV-treated group (Figure 4B), which may be the result of innate immune cells activation. Future studies will utilize non-immune compromised mouse models to investigate the possibility of immuno-chemo combination therapies delivered through plant virus-based delivery.

CONCLUSION

Tobacco mosaic viral encapsulation of phenanthriplatin enables therapy in a mouse model of triple negative breast cancer. Although each nanoparticle platform technology, synthetic and natural, has advantages and disadvantages, we would like to highlight benefits of the plant viral approach. Harnessing the nucleoprotein components of viruses for medical cargo delivery is an important advantage compared to mammalian viral vector systems. Plant viruses are not virulent in animal cells.[30,31] Other benefits include the relative ease of synthesis and purification, resulting in highly monodisperse products with predictable surface morphologies. Quality control and assurance processes are critical. One of the strengths of plant virus-based platforms is the ease of virus production with subunits that are genetically controlled. To a first approximation, every particle is identical. Our data demonstrate high reproducibility of the PhenPt-TMV nanomanufacturing process. Combined with its enhanced *in vivo* efficacy and successful delivery to cancer cells, the present approach is a most promising drug delivery discovery.

MATERIALS AND METHODS

Synthesis of PhenPt-TMV

Established protocols were used to produce TMV in *Nicotiana benthamiana* plants[15] and synthesize phenanthriplatin.[4] Phenanthriplatin was allowed to react with $AgNO_3$ to give the aquated species (Figure 1), which was then mixed with TMV using a 17,000-fold excess of aquated phenanthriplatin in 10 mM potassium phosphate buffer pH 7.8. Protein concentration was kept at 1 mg/mL, and the reaction was stopped after 30 min. The PhenPt–TMV complex was purified over a 40% (w/v) sucrose cushion at 160,000 *g* for 3 h and resuspended in sterile PBS. The concentration of TMV was determined by UV–vis spectroscopy,[15] and the platinum content was measured using ICP-MS. Structural integrity

was confirmed by transmission electron microscopy, dynamic light scattering, and zeta potential measurement.

Cell Uptake and Cytotoxicity

Cell uptake was monitored by using MDA-MB-231 cells, a generous gift from Dr. Schiemann, Case Western Reserve University, and sulfo-Cy5 fluorescently labeled TMV and flow cytometry methods were as previously described.[11] Data were recorded with a BD LSRII flow cytometer and analyzed using FlowJo 8.63 software. The intracellular distribution of phenanthriplatin and PhenPt-TMV was determined following a 24 h incubation with A2780 cells. Cell components were separated by using a commercially available kit (Thermo Scientific NE-PER Nuclear and Cytoplasmic Extraction Kit) and atomic absorption spectroscopy as previously described. Efficacy was analyzed by using the MTT assay (ATCC) and a panel of human cancer cell lines: A2780 (ovarian cancer), A2780/CP70 (ovarian cancer resistant to cisplatin), OV81.2 (ovarian cancer, primary patient cells; cells were a generous gift from Dr. DiFeo, Case Western Reserve University), 8988T (pancreatic 375 cancer) cells were a generous gift from Dr. Ghoroghchian, MIT. LNCAP (prostate cancer), MCF-7 (breast cancer), MDA-MB231 (breast cancer) cells were obtained from ATCC unless indicated otherwise. The assay was performed as per manufacturer's recommendation; a BioTek Synergy HT multidetection microplate reader was used for read-out.

Intracellular Trafficking

Intracellular trafficking was monitored in MDA-MB-231 cells; 25,000 cells were seeded overnight on glass coverslips and incubated for 8 h with 1×10^6 TMV particles per cell. Following incubation, cells were washed, fixed, and stained. Cell membrane was stained using wheat germ agglutinin conjugated to AlexaFluor 555. TMV was stained using a rabbit anti-TMV antibody primary and a goat antirabbit secondary conjugated to AlexaFluor 647. Endolysosomes were stained using a mouse antihuman Lamp-1 antibody primary and a goat antimouse secondary conjugated to AlexaFluor 488. Slides were imaged using Zeiss Axio Imager Z1 fluorescent inverted high-resolution microscope with motorized stage.

In Vivo Phenanthriplatin Delivery Using the MDA-MB-231 Model

All animal studies were carried using IACUC-approved procedures. NCR nu/nu mice were injected subcutaneously into the right flank using 2×10^6 MDA-MB-231 cells suspended in 100 μL of media and Matrigel (Corning) at a 1:1 ratio. Once established, tumors were monitored daily, and treatment was started when tumors reached 250–300 mm^3. Two independent studies with $n = 5$ animals per groups were performed. Treatment was administered intravenously at weekly intervals at a dosage of 1.0 mg/kg body weight phenanthriplatin. Groups were treated with phenanthriplatin, PhenPt-TMV, TMV, cisplatin, and PBS. PhenPt-TMV was prepared fresh, and platinum content was determined immediately prior to every injection. The dosage was normalized to platinum or TMV content. Tumors were measured daily and total volume was calculated using the formula: $v = \frac{l \times w^2}{2}$. Mice were weighed every other day to monitor potential side effects. Mice were euthanized following 30 days of treatment or as determined by IACUC guidelines.

Hematoxylin and eosin staining was performed according to previously described methods[32] and imaged using Zeiss Axio Imager Z1 fluorescent inverted high resolution microscope with motorized stage.

Biodistribution

Cy5-labeled PhenPt-TMV and free PhenPt (at 1.0 mg/kg) were administered intravenously into MDA-MB-231 tumor bearing mice. Mice were euthanized after 24 h and imaged using the Maestro fluorescence imaging system. Organs were removed and imaged individually and ROIs were evaluated. Platinum content in each organ was extracted and determined using graphite furnace atomic absorption spectroscopy (GFAAS).

Liver and Kidney Toxicity

Balb/c mice ($n = 3$) were injected with 100 μL PBS, TMV, phenanthriplatin, or PhenPt-TMV at the same dosage administered for the efficacy studies (normalized to 1.0 mg/kg body weight phenanthriplatin). After 24 h, blood was collected via retro-orbital bleeds and tested for ALT and AST activity levels using commercially available kits (Sigma-Aldrich). Animals were then euthanized, and livers and kidneys were paraffin-embedded, sectioned, and stained as described above.

Acknowledgments

This work was supported in part by grants from the National Cancer Institute (CA 034992 to S.J.L.), National Science Foundation (CHE 1306447 to N.F.S.), and Mt. Sinai Foundation (to N.F.S.). A.E.C. was supported in part by NIH grants T32 GM007250 and TL1 TR000441. We thank Case Western Reserve University Farm for support in scaled-up molecular farming.

References

1. Yao X, Panichpisal K, Kurtzman N, Nugent K. Cisplatin Nephrotoxicity: A Review. Am J Med Sci. 2007; 334:115–124. [PubMed: 17700201]
2. Cooke SL, Brenton JD. Evolution of Platinum Resistance in High-Grade Serous Ovarian Cancer. Lancet Oncol. 2011; 12:1169–1174. [PubMed: 21742554]
3. White SC, Lorigan P, Margison GP, Margison JM, Martin F, Thatcher N, Anderson H, Ranson M. Phase II Study of SPI-77 (Sterically Stabilised Liposomal Cisplatin) in Advanced Non-Small-Cell Lung Cancer. Br J Cancer. 2006; 95:822–828. [PubMed: 16969346]
4. Park GY, Wilson JJ, Song Y, Lippard SJ. Phenanthriplatin, a Monofunctional DNA-Binding Platinum Anticancer Drug Candidate with Unusual Potency and Cellular Activity Profile. Proc Natl Acad Sci U S A. 2012; 109:11987–11992. [PubMed: 22773807]
5. Kellinger MW, Park GY, Chong J, Lippard SJ, Wang D. Effect of a Monofunctional Phenanthriplatin-DNA Adduct on RNA Polymerase II Transcriptional Fidelity and Translesion Synthesis. J Am Chem Soc. 2013; 135:13054–13061. [PubMed: 23927577]
6. Gregory MT, Park GY, Johnstone TC, Lee YS, Yang W, Lippard SJ. Structural and Mechanistic Studies of Polymerase η Bypass of Phenanthriplatin DNA Damage. Proc Natl Acad Sci U S A. 2014; 111:9133–9138. [PubMed: 24927576]
7. Johnstone TC, Park GY, Lippard SJ. Understanding and Improving Platinum Anticancer Drugs–Phenanthriplatin. Anticancer Res. 2014; 34:471–476. [PubMed: 24403503]
8. Liu TC, Galanis E, Kirn D. Clinical Trial Results with Oncolytic Virotherapy: A Century of Promise, a Decade of Progress. Nat Clin Pract Oncol. 2007; 4:101–117. [PubMed: 17259931]
9. Giacca M, Zacchigna S. Virus-Mediated Gene Delivery for Human Gene Therapy. J Controlled Release. 2012; 161:377–388.

10. Bruckman MA, Randolph LN, Vanmeter A, Hern S, Shoffstall AJ, Taurog RE, Steinmetz NF. Biodistribution, Pharmacokinetics, and Blood Compatibility of Native and Pegylated Tobacco Mosaic Virus Nano-Rods and -Spheres in Mice. Virology. 2014; 449:163–173. [PubMed: 24418549]
11. Shukla S, Eber FJ, Nagarajan AS, DiFranco NA, Schmidt N, Wen AM, Eiben S, Twyman RM, Wege C, Steinmetz NF. The Impact of Aspect Ratio on the Biodistribution and Tumor Homing of Rigid Soft-Matter Nanorods. Adv Healthcare Mater. 2015; 4:874–882.
12. Geng Y, Dalhaimer P, Cai S, Tsai R, Tewari M, Minko T, Discher DE. Shape Effects of Filaments *Versus* Spherical Particles in Flow and Drug Delivery. Nat Nanotechnol. 2007; 2:249–255. [PubMed: 18654271]
13. Chauhan VP, Popović Z, Chen O, Cui J, Fukumura D, Bawendi MG, Jain RK. Fluorescent Nanorods and Nanospheres for Real-Time *in Vivo* Probing of Nanoparticle Shape-Dependent Tumor Penetration. Angew Chem, Int Ed. 2011; 50:11417–11420.
14. Bruckman M, Jiang K, Simpson EJ, Randolph L, Luyt LG, Yu X, Steinmetz NF. Dual-Modal Magnetic Resonance and Fluorescence Imaging of Atherosclerotic Plaques *in Vivo* Using VCAM-1 Targeted Tobacco Mosaic Virus. Nano Lett. 2014; 14:1551–1558. [PubMed: 24499194]
15. Bruckman MA, Steinmetz NF. Chemical Modification of the Inner and Outer Surfaces of Tobacco Mosaic Virus (TMV). Methods Mol Biol. 2014; 1108:173–185. [PubMed: 24243249]
16. Klug A. The Tobacco Mosaic Virus Particle: Structure and Assembly. Philos Trans R Soc, B. 1999; 354:531–535.
17. Bruckman MA, Hern S, Jiang K, Flask CA, Yu X, Steinmetz NF. Tobacco Mosaic Virus Rods and Spheres as Supramolecular High-Relaxivity MRI Contrast Agents. J Mater Chem B. 2013; 1:1482–1490.
18. Brunel FM, Lewis JD, Destito G, Steinmetz NF, Manchester M, Stuhlmann H, Dawson PE. Hydrazone Ligation Strategy to Assemble Multifunctional Viral Nanoparticles for Cell Imaging and Tumor Targeting. Nano Lett. 2010; 10:1093–1097. [PubMed: 20163184]
19. Wu Z, Chen K, Yildiz I, Dirksen A, Fischer R, Dawson PE, Steinmetz NF. Development of Viral Nanoparticles for Efficient Intracellular Delivery. Nanoscale. 2012; 4:3567–3576. [PubMed: 22508503]
20. Du J, Lane LA, Nie S. Stimuli-Responsive Nanoparticles for Targeting the Tumor Microenvironment. J Controlled Release. 2015; 219:205–214.
21. Behrens BC, Hamilton TC, Masuda H, Grotzinger KR, Whang-Peng J, Louie KG, Knutsen T, McKoy WM, Young RC, Ozols RF. Characterization of a Cis-Diamminedichloroplatinum-(II)-Resistant Human Ovarian Cancer Cell Line and Its Use in Evaluation of Platinum Analogues. Cancer Res. 1987; 47:414–418. [PubMed: 3539322]
22. Nagaraj AB, Joseph P, Kovalenko O, Singh S, Armstrong A, Redline R, Resnick K, Zanotti K, Waggoner S, DiFeo A. Critical Role of Wnt/β-Catenin Signaling in Driving Epithelial Ovarian Cancer Platinum Resistance. Oncotarget. 2015; 6:23720–23734. [PubMed: 26125441]
23. Aljabali AA, Shukla S, Lomonossoff GP, Steinmetz NF, Evans DJ. CPMV-Dox Delivers. Mol Pharmaceutics. 2013; 10:3–10.
24. Wen AM, Infusino M, De Luca A, Kernan DL, Czapar AE, Strangi G, Steinmetz NF. Interface of Physics and Biology: Engineering Virus-Based Nanoparticles for Biophotonics. Bioconjugate Chem. 2015; 26:51–62.
25. Maeda H, Wu J, Sawa T, Matsumura Y, Hori K. Tumor Vascular Permeability and the EPR Effect in Macromolecular Therapeutics: A Review. J Controlled Release. 2000; 65:271–284.
26. Lee KL, Shukla S, Wu M, Ayat NR, El Sanadi CE, Wen AM, Edelbrock JF, Pokorski JK, Commandeur U, Dubyak GR, Steinmetz NF. Stealth Filaments: Polymer Chain Length and Conformation Affect the *in Vivo* Fate of Pegylated Potato Virus X. Acta Biomater. 2015; 19:166–179. [PubMed: 25769228]
27. LeBond, RF.; DDB; Suneja, M.; Szot, JF.; DeGowin, EL. DeGowin's Diagnostic Examination. 10. McGraw-Hill Education/Medical; New York: 2015. Common Laboratory Tests.
28. Miller MA, Zheng YR, Gadde S, Pfirschke C, Harshal Z, Engblom C, Kohler RH, Iwamoto Y, Yang KS, Askevold B, Kolishetti N, Pittet M, Lippard SJ, Farokhzad OC, Weissleder R. Tumour-

associated macrophages act as a slow-release reservoir of nano-therapeutic Pt(IV) pro-drug. Nat Commun. 2015; 6:8692. [PubMed: 26503691]

29. Lizotte PH, Wen AM, Sheen MR, Fields J, Rojanasopondist P, Steinmetz NF, Fiering S. *In Situ* Vaccination with Cowpea Mosaic Virus Nanoparticles Suppresses Metastatic Cancer. Nat Nanotechnol. 2015; 11:295–303. [PubMed: 26689376]
30. Kaiser CR, Flenniken ML, Gillitzer E, Harmsen AL, Harmsen AG, Jutila MA, Douglas T, Young MJ. Biodistribution Studies of Protein Cage Nanoparticles Demonstrate Broad Tissue Distribution and Rapid Clearance *in Vivo*. Int J Nanomed. 2007; 2:715–733.
31. Yildiz I, Shukla S, Steinmetz NF. Applications of Viral Nanoparticles in Medicine. Curr Opin Biotechnol. 2011; 22:901–908. [PubMed: 21592772]
32. Fischer AH, Jacobson KA, Rose J, Zeller R. Hematoxylin and Eosin Staining of Tissue and Cell Sections. Cold Spring Harbor Protoc. 2008; 2008 pdb.prot4986.

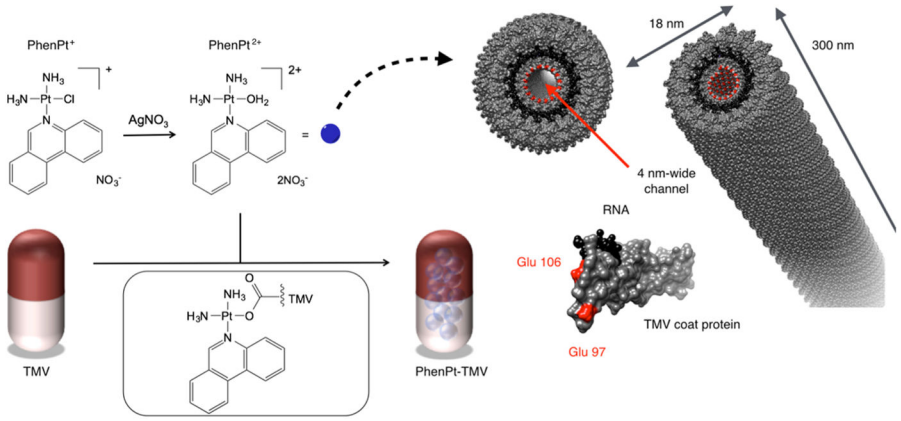

Figure 1.

Loading scheme and structures of phenanthriplatin and PhenPt-TMV, where PhenPt-TMV is prepared by nanoencapsulation of $PhenPt^{2+}$ within the virus. Structure of tobacco mosaic virus (TMV, images were created using Chimera software and PDB entry TMV2); the TMV coat protein and assembled hollow nanotube are shown in cross-sectional and longitudinal orientations. The coat protein is depicted in gray, the RNA in black, and interior glutamic acids Glu 97 and Glu 106 are highlighted in red.

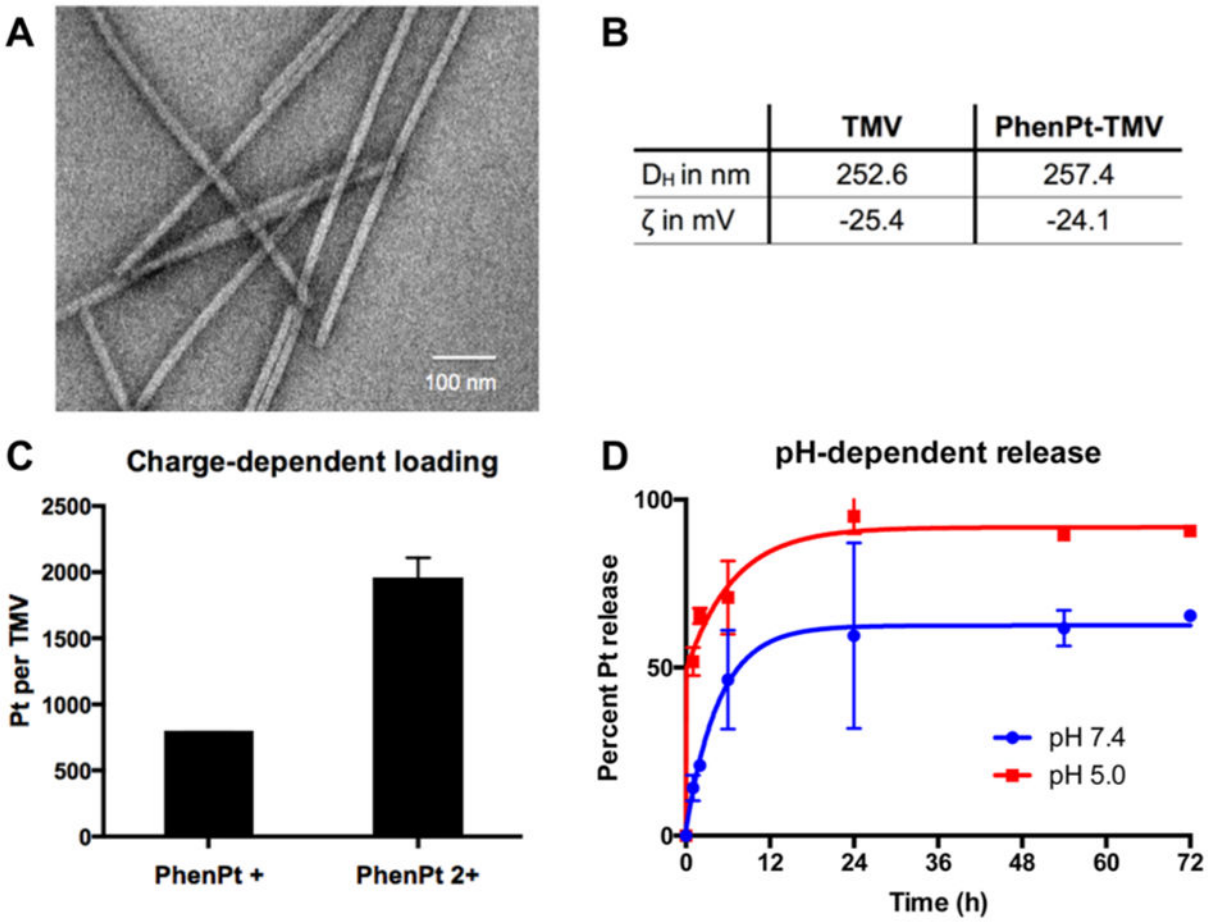

Figure 2.

Characterization of PhenPt-TMV. See Materials and Methods for synthetic details. (A) TEM images of negative-stained PhenPt-TMV coated grids. (B) Hydrodynamic diameter (D_H) measured by dynamic light scattering and zeta potential (ζ) of TMV and PhenPt-TMV. (C) Platinum content per TMV after encapsulation of phenanthriplatin and its aquated form measured by ICP-MS. (D) Percent phenanthriplatin release from TMV over time in PBS at 7.4 (blue) and acetate buffer at 5.0 (red).

A

Cell line	Cancer type	IC_{50} in μM		
		Cisplatin	PhenPt	PhenPt-TMV
MDA-MB231	Breast	>20	3.05	2.21
MCF-7	Breast	>20	3.59	2.59
A2780	Ovarian	0.88	0.56	0.29
A2780/DDP	Ovarian, cisplatin resistant	>20	2.05	1.52
OV81.2	Ovarian, primary patient cells	3.58	0.68	0.67
8988T	Pancreatic	>20	1.07	1.66

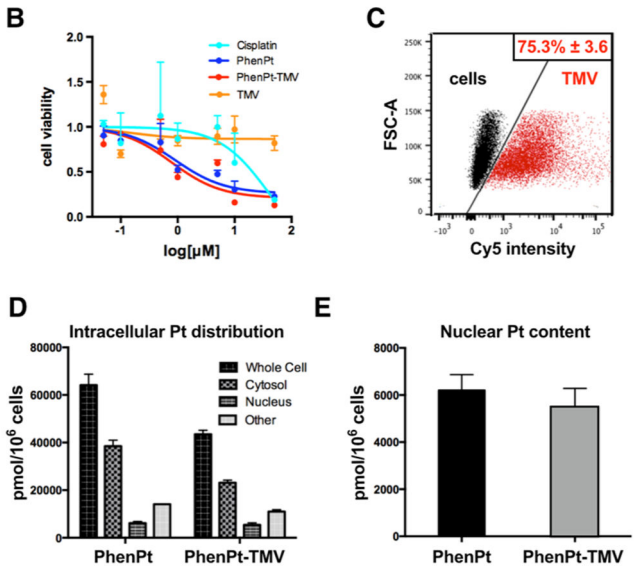

Figure 3.

Cellular uptake and efficacy of PhenPt-TMV *in vitro*. (A) IC_{50} values for cisplatin, free phenanthriplatin (PhenPt), and PhenPt-TMV in a six-cell line panel as determined by MTT assays. (B) MTT assay using MDA-MB-231 cells. (C) Flow cytometry of MDA-MB-231 cells without treatment and following 3 h incubation with Cy5-labeled TMV. (D,E) Intracellular distribution and nuclear content of platinum in A2780 cells following 24-h incubation with free phenanthriplatin and PhenPt-TMV.

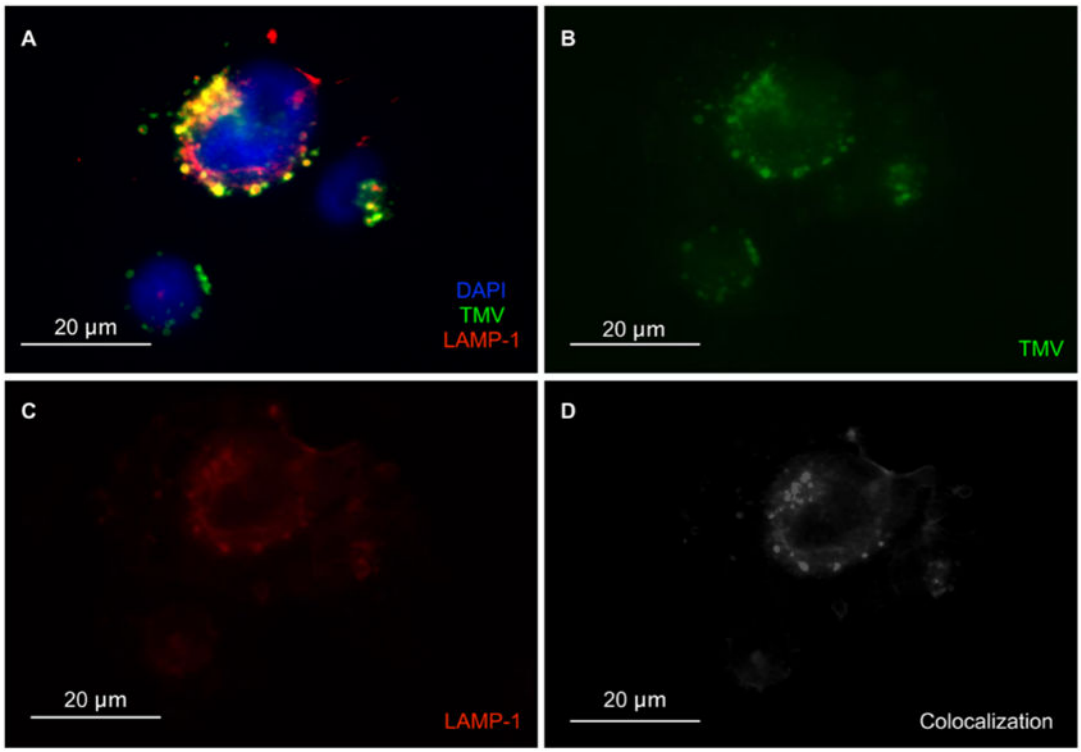

Figure 4.

Cellular trafficking of TMV within MDA-MB-231 cells. (A) Composite image of TMV in MDA-MB-231 cells at 8 h post incubation. TMV is shown in green (immunostained using rabbit anti-TMV) (B), nuclei in blue (stained with DAPI), and endolysosomes in red (stained with Lamp-1) (C). (D) Co-localization analysis using the “co-localization highlight” plug-in and ImageJ software. White = co-localization of TMV and Lamp-1.

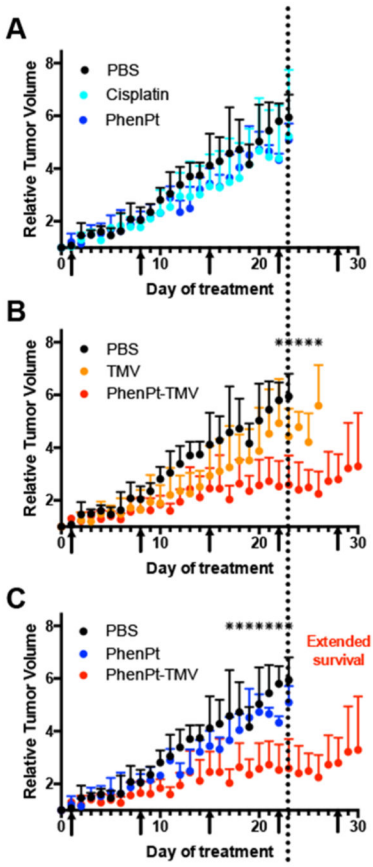

Figure 5.

Treatment of MDA-MB-231 xenografts in an athymic mouse model. Treatment begun when tumors reached 250–300 mm^3; arrows indicate the treatment schedule; treatment was given by an intravenous bolus injection of 1.0 mg/kg of PhenPt-TMV, phenanthriplatin (PhenPt), cisplatin, TMV, or PBS; dosage was normalized to platinum content. Tumor volumes were monitored daily, and total volume was normalized to initial tumor size at time of treatment. Each treatment group consists of 5 animals ($n = 5$); * indicates $p < 0.05$. (A) cisplatin vs phenanthriplatin, (B) PhenPt-TMV vs TMV, and (C) PhenPt-TMV vs phenanthriplatin.

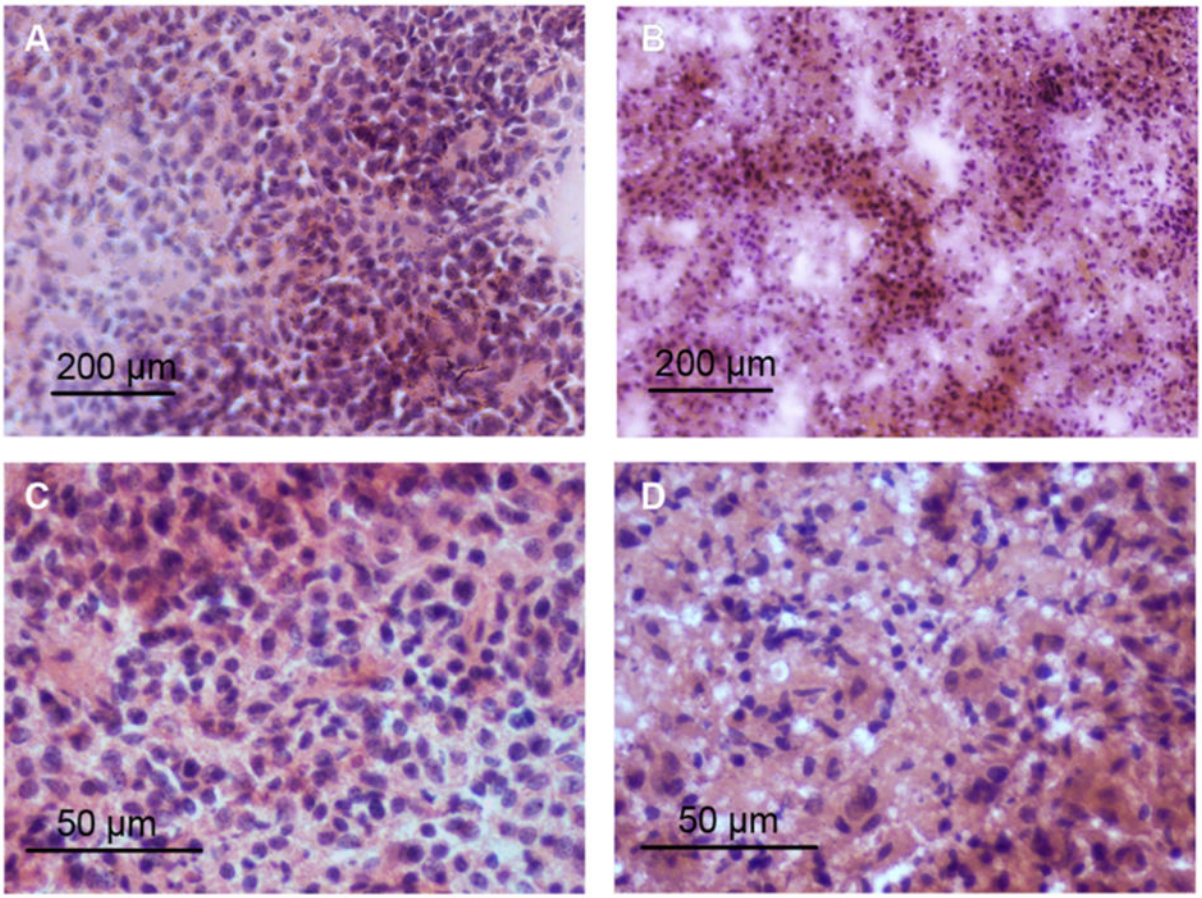

Figure 6.

Histology of MDA-MB-231 tumor sections. H&E-stained tumor tissue sections from (A,C) PBS treated and (B,D) PhenPt-TMV treated animals. Tumors were collected and stained at the completion of the treatment.

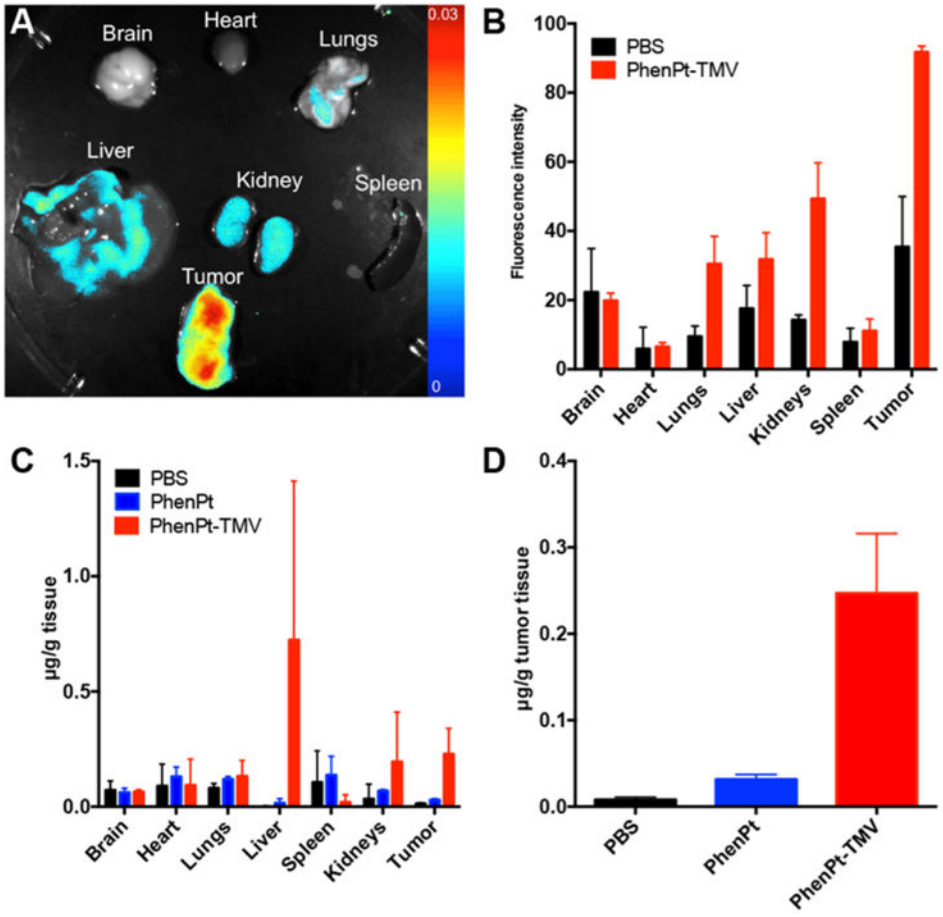

Figure 7.

Biodistribution of PhenPt-TMV in MDA-MB-231 tumor bearing animals. (A) Representative Maestro imaging of excised organs 24 h after administration Cy5-labeled PhenPt-TMV. (B) Quantitative ROI analysis of excised organs from (A) quantifying average fluorescence intensity (tissues from $n = 3$ animals were analyzed). (C,D) Platinum concentration in organ tissue as measured by atomic absorption spectroscopy 24 h post-administration of phenanthriplatin or PhenPt-TMV followed by tissue homogenization.

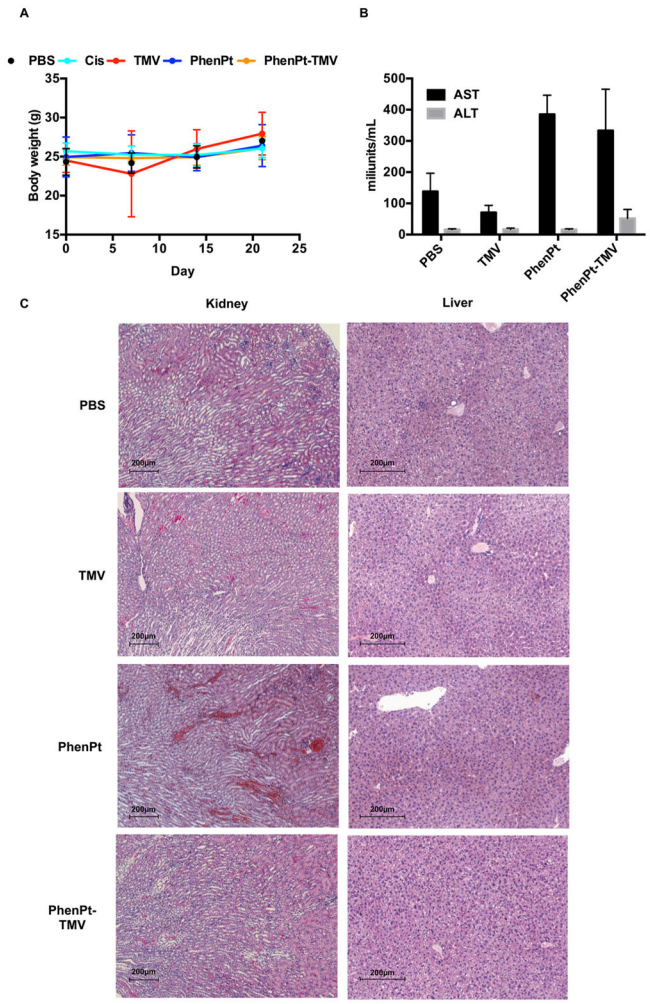

Figure 8.

Toxicity of PhenPt-TMV in treated animals. (A) Weight of treated tumor bearing mice over the course of the study. (B) AST and ALT liver enzyme testing 24 h following administration of PBS, TMV, phenanthriplatin, or PhenPt-TMV. (C) H&E stained liver and kidney tissue from mice 24 h following administration of PBS, TMV, phenanthriplatin, or PhenPt-TMV.